Available online at www.sciencedirect.com
SCIENCE DIRECT®
International Journal of Heat and Fluid Flow 24 (2003) 412–420
International Journal of HEAT AND FLUID FLOW
www.elsevier.com/locate/ijhff

Large eddy simulation of turbulent flow in a rotating pipe

A.A. Feiz, M. Ould-Rouis *, G. Lauriat

LETEM, Université de Marne-la-Vallée, Bât. Lavoisier, 77454 Marne-la-Vallée Cedex 2, France

Received 19 January 2002; accepted 7 December 2002

Abstract

Large eddy simulation (LES) of fully developed, incompressible turbulent channel flows are presented for stationary and rotating pipes. A dynamic model and the Smagorinsky model were used and compared with DNS results. The 3-D governing equations written in a cylindrical coordinate system were solved by a finite difference method, second-order accurate in space and in time. The features of the flows at two Reynolds numbers and for various rotation speeds are discussed and compared to available data of literature.
© 2003 Published by Elsevier Science Inc.

Keywords: Rotating pipe; Turbulent flow; Large eddy simulation

1. Introduction

Turbulent circular pipe flows have attracted the interest of many investigators. The simplest case of non-rotating pipe has been extensively studied experimentally (Laufer, 1954; Lawn, 1971) and numerically. Most of the numerical simulations were focused on the flow stability and transition regime (Itoh, 1977; Patera and Orszag, 1981). Some direct numerical simulations (DNS) have also been performed. Using mixed finite-difference and spectral methods, Nikitin (1993) obtained satisfactory agreement with experimental data within a range of Reynolds number from 2250 to 5900. Unger et al. (1993) obtained excellent agreement with experiments, using a second order accurate finite-difference method, and confirmed that pipe flow at the lowest range of turbulent Reynolds number deviates from the universal logarithmic law. Zhang et al. (1994) presented simulations of turbulent pipe flows at moderate Reynolds number by using a 3-D spectral code. Their results agree satisfactorily with experiments and previous numerical simulations. Eggels et al. (1994b) have carried out DNS and experiments in order to investigate the differences between fully developed turbulent flow in circular and plane channels, and concluded that most of the statistics on fluctuating velocities are marginally affected by the axisymmetry of the duct geometry.

When a fluid enters a rotating pipe, a tangential component of velocity is brought by the moving wall and the flow exhibits a complicated three-dimensional behaviour. The high levels of turbulence and large shearing rates associated with swirling flows enhance the mixing process and provide a more homogeneous flow fluids. Recently, numerical simulation of turbulent rotating pipe flow has received some interest. For example, Eggels et al. (1994a) used a DNS of the turbulent rotating pipe flow for moderate values of the rotation number, N, and confirmed that the drag is reduced as it has been observed experimentally. Orlandi and Fatica (1997) performed also DNS of turbulent rotating pipe flows for rotation number out of the range considered by Eggels et al. (1994a) but not high enough to include a re-laminarization of the flow, and to analyse the modifications of the near-wall vortical structures. They showed that a degree of drag reduction is achieved in the numerical simulations like in the experiments, and that the changes in turbulence statistics are due to the tilting of the near-wall streamwise vortical structures in the direction of rotation. In the more recent study by Orlandi and Ebstein (2000), N has been increased up to 10 and the budgets for the Reynolds stresses were evaluated; these budgets being of great importance in

* Corresponding author.
E-mail address: ould@univ-mlv.fr (M. Ould-Rouis).

0142-727X/03/$ - see front matter © 2003 Published by Elsevier Science Inc.
doi:10.1016/S0142-727X(02)00241-2

Nomenclature

L_z	length of the computational domain
N	rotation number
r	dimensionless coordinate in radial direction scaled by the pipe radius
R	pipe radius (m)
S_{ij}	rate of strain tensor
u_τ	shear stress velocity
$U_b = U_p/2$	bulk velocity
U_p	centreline streamwise velocity of the laminar Poiseuille flow
v'_r, v'_θ, v'_z	fluctuating velocity components
$\langle v'_r v'_z \rangle$	one of the six Reynolds stress components
y	dimensionless distance from the wall, $y = 1 - r$
$y^+ = (1-r)u_\tau/\nu$	distance from the wall in viscous wall units
z	coordinate in axial direction

Greeks

$\Delta = (r\Delta r\Delta\theta\Delta z)^{1/3}$	characteristic gridspacing
Δr	gridspacing in radial direction
$\Delta\theta$	gridspacing in circumferential direction
Δz	gridspacing in axial direction
ν	kinematic viscosity
θ	coordinate in circumferential direction

the development of improved one-closure turbulence models applied to rotating flows.

Investigations devoted to LES of turbulent pipe flow are very few in the literature. The first LES work on fully developed turbulent pipe flow was by Unger and Friedrich (1991). LES have been applied to flows in complex geometries to a very limited extent. The major reasons for this are due to the difficulty in describing non-trivial geometries accurately whilst limiting the number of computational grid points. LES predictions on turbulent pipe flow with rotation are extremely scarce. Eggels and Nieuwstadt (1993) used a Smagorinsky model and showed that their numerical results compared reasonably well with experimental data. More recently, Yang and McGuirk (1999) examined by using LES the effects of swirl driven by the rotating wall, and their numerical results compare reasonably well with the measurements of Imao and Itoh (1996). However, the performance of the dynamic subgrid scale model was only slightly better than that of the Smagorinsky model in their study. They pointed out that the reason may be the use of a too fine mesh. They have confirmed numerically by LES the experimental observations that turbulence decreases with an increase in pipe rotation due to the stabilizing effect of the centrifugal force.

In this study, we present results for LES of a rotating pipe flow at moderate Reynolds numbers ($Re = 4900$ and $Re = 7400$). The numerical results are compared to simulations obtained for the same Reynolds number, namely the DNS by Orlandi and Fatica (1997) which compare reasonably well with available experimental data. The main objective of this work is to study fully turbulent rotating pipe flow by LES and to assess the performances of two different subgrid scale models (a dynamic model and the Smagorinsky model) for swirling flows, in particular to examine whether the effects of swirl driven by the rotating wall are properly captured by LES.

2. Basic equations and numerical procedure

The governing equations for an incompressible, newtonian fluid flow (3D Navier–Stokes equations) are cast in terms of the new variables $q_r = r.v_r$, $q_\theta = v_\theta$ and $q_z = v_z$ to avoid the singularity at the axis $r = 0$ (Fig. 1). The dimensionless equations in a cylindrical polar coordinate system using U_p, the centreline streamwise velocity of the laminar Poiseuille flow, and the pipe radius R as velocity and length scales, respectively, have the form:

$$\frac{\partial \overline{q_r}}{\partial r} + \frac{\partial \overline{q_\theta}}{\partial \theta} + r\frac{\partial \overline{q_z}}{\partial z} = 0$$

$$\frac{\partial \overline{q_\theta}}{\partial t} + \frac{1}{r^2}\frac{\partial r\overline{q_\theta}\,\overline{q_r}}{\partial r} + \frac{\partial \overline{q_\theta}\,\overline{q_\theta}}{\partial \theta} + \frac{\partial \overline{q_\theta}\,\overline{q_z}}{\partial z} + N\overline{q_r} = -\frac{1}{r}\frac{\partial \overline{P}}{\partial \theta} + \frac{1}{Re}\left[\frac{1}{r^2}\frac{\partial r^2\hat{\tau}_{r\theta}}{\partial r} + \frac{1}{r}\frac{\partial \hat{\tau}_{\theta\theta}}{\partial \theta} + \frac{\partial \hat{\tau}_{z\theta}}{\partial z}\right],$$

$$\frac{\partial \overline{q_r}}{\partial t} + \frac{\partial}{\partial r}\left(\frac{\overline{q_r}\,\overline{q_r}}{r}\right) + \frac{\partial}{\partial \theta}\left(\frac{\overline{q_\theta}\,\overline{q_r}}{r}\right) + \frac{\partial \overline{q_r}\,\overline{q_z}}{\partial z} - \overline{q_\theta}\,\overline{q_\theta} = Nr\overline{q_\theta} - r\frac{\partial \overline{P}}{\partial r} + \frac{1}{Re}\left[\frac{\partial r\hat{\tau}_{rr}}{\partial r} + \frac{\partial \hat{\tau}_{r\theta}}{\partial \theta} + r\frac{\partial \hat{\tau}_{rz}}{\partial z} - \hat{\tau}_{\theta\theta}\right],$$

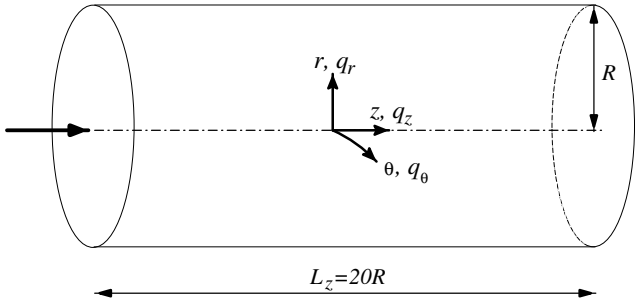

Fig. 1. Schematic of turbulent flow in an axially rotating circular pipe.

$$\frac{\partial \overline{q_z}}{\partial t}+\frac{1}{r}\frac{\partial \overline{q_r}\,\overline{q_z}}{\partial r}+\frac{1}{r}\frac{\partial \overline{q_\theta}\,\overline{q_z}}{\partial \theta}+\frac{\partial \overline{q_z}\,\overline{q_z}}{\partial z}$$
$$=-\frac{\partial \overline{P}}{\partial z}+\frac{1}{Re}\left[\frac{1}{r}\frac{\partial r\hat{\tau}_{rz}}{\partial r}+\frac{1}{r}\frac{\partial \hat{\tau}_{z\theta}}{\partial \theta}+\frac{\partial \hat{\tau}_{zz}}{\partial z}\right].$$

The dimensionless numbers are the Reynolds number, $Re = 2U_bR/\nu$, and the rotation number, $N = \Omega R/U_b$ (related to Rossby number by $N = 1/Ro$). A mean pressure gradient in the q_z equation maintains a constant bulk velocity U_b. The total stresses $\hat{\tau}_{ij} = \overline{\tau_{ij}} + \tau'_{ij}$ are $\hat{\tau}_{ij} = (1 + \nu_T Re)\overline{S_{ij}}$ where the strain tensor expressed by the variables q_i is:

$$\begin{pmatrix} S_{\theta\theta} & S_{r\theta} & S_{z\theta} \\ S_{r\theta} & S_{rr} & S_{rz} \\ S_{z\theta} & S_{rz} & S_{zz} \end{pmatrix}$$
$$= \begin{pmatrix} \left[\frac{1}{r}\frac{\partial q_\theta}{\partial \theta}+\frac{q_r}{r^2}\right] & \frac{1}{2}\left[r\frac{\partial (q_\theta/r)}{\partial r}+\frac{1}{r^2}\frac{\partial q_r}{\partial \theta}\right] & \frac{1}{2}\left[\frac{1}{r}\frac{\partial q_z}{\partial \theta}+\frac{\partial q_\theta}{\partial z}\right] \\ S_{r\theta} & \frac{\partial (q_r/r)}{\partial r} & \frac{1}{2}\left[\frac{1}{r}\frac{\partial q_r}{\partial z}+\frac{\partial q_z}{\partial r}\right] \\ S_{z\theta} & S_{rz} & \frac{\partial q_z}{\partial z} \end{pmatrix}.$$

The eddy viscosity ν_T has different expressions according to the subgrid model used.

2.1. Smagorinsky model

In this model, the subgrid scale eddy viscosity is related to the deformation of the resolved velocity field as:

$$\nu_T = (C_S\Delta)^2|\overline{S}| = (C_S\Delta)^2[2\overline{S_{ij}}\,\overline{S_{ij}}]^{1/2}$$

In the present study, the Smagorinsky coefficient C_S is set equal to 0.15. For a discussion on the value and the interpretation of this constant, we refer to Mason and Callen (1986). This subgrid model largely used in LES of isotropic turbulence produced good results. When applied to inhomogeneous, and in particular to wall bounded flows, the constant was modified.

2.2. Dynamic eddy viscosity model

The dynamic model provides a methodology for determining an appropriate local value of the Smagorinsky coefficient. The model was proposed by Germano et al. (1991), with important modifications and extensions provided by Lilly (1992). In this model, the constant C_d is not given a priori, but is computed during the simulation from the flow variables. The turbulent viscosity is expressed using an eddy viscosity assumption as:

$$\nu_T = C_d(\Delta^2)\left[2\overline{S_{ij}}\,\overline{S_{ij}}\right]^{1/2}$$

C_d is dynamically determined as follows.

Two different filter widths are introduced; the test filter $\widetilde{\Delta}$ is larger than the computational filter Δ and it is applied to the momentum equations. Germano et al. (1991) derived an exact relationship between the subgrid scale stress tensors at the two different filter widths (Germano identity). Substitution of a Smagorinsky form $|S| = \sqrt{2S_{ij}S_{ij}}$ for the subgrid scale stress into Germano identity, along with some additional assumptions (Lilly, 1992), leads to the following expression for C_d:

$$C_d = -\frac{1}{2\Delta^2}\frac{\langle L_{ij}M_{ij}\rangle}{\langle M_{ij}M_{ij}\rangle} \tag{1}$$

where the second order tensors L_{ij} and M_{ij} are given as follows:

$$L_{ij} = \widetilde{\overline{q}_i\overline{q}_j} - \tilde{\overline{q}}_i\tilde{\overline{q}}_j = -2C_d\Delta^2 M_{ij}, \quad M_{ij} = \frac{\widetilde{\Delta^2}}{\Delta^2}|\widetilde{\overline{S}}|\widetilde{\overline{S}_{ij}} - |\widetilde{\overline{S}}|\widetilde{\overline{S}_{ij}}$$

Positive values of C_d are linked to energy flowing from large to small scales and negative values to energy going from small to large scales (backward energy transfer). The angled brackets in Eq. (1) denotes averages in the homogeneous direction.

2.3. Numerical procedures

The governing equations were discretized on a staggered mesh in cylindrical coordinates. The solutions were obtained by using a finite difference scheme, second-order accurate in space and in time, based on a fractional-step method. The advancement in time is accomplished by a third-order Runge–Kutta explicit scheme for the non-linear term while the viscous term employs a Crank–Nicholson implicit scheme. Uniform computational grid and periodic boundary conditions were applied to the circumferential and axial directions. In the radial direction, non-uniform meshes specified by a hyperbolic tangent function were employed. On the pipe wall, the usual no-slip boundary condition is applied.

Most of the computations for a pipe of length $L_z = 20R$ were performed using a $65 \times 39 \times 65$ grid but the influence of the grid resolution on the accuracy of the solution was investigated. The finest grid ($129 \times 49 \times 129$) leads to well resolved simulations. However, the $65 \times 39 \times 65$ grid predicts and captures all of the features of the flow although small differences occur between some of the statistics obtained with these two grids. Since, the fine grid requires much larger CPU-time and storage requirements, we performed simulations on the $65 \times 39 \times 65$ grid which gives a good compromise between CPU-time and accuracy. The final statistics are accumulated by spatial averaging in the homogeneous streamwise and circumferential directions and by time-averaging. The runs with the Smagorinsky subgrid scale model and a dynamic subgrid scale model have been carried out for the non-rotating pipe wall and for the rotating pipe wall at two rotation rates, $N = 1$ and $N = 2$, and at two Reynolds numbers, $Re = 4900$ and $Re = 7400$.

3. Results and discussion

The axial mean velocity profile is plotted in Fig. 2 versus the dimensionless distance from the wall for various rotation numbers ($N = 0, 1, 2$). When the pipe is rotating the streamwise velocity increases near the centre and decreases near the wall. The computational mean velocity profile gradually approaches a Poiseuille profile, due to the stabilizing effect of the centrifugal force. This laminarization phenomena is the deformation of the axial velocity profile into a shape similar to the laminar one, and the decrease of the friction factor caused by the pipe rotation. This observation has been reported by other investigators (Nishibori et al., 1987; Hirai et al., 1988). Therefore, rotation has a very marked influence on the damping of the turbulent motion and on the drag reduction (see experiments by Nishibori et al., 1987, Reich and Beer, 1989, Imao and Itoh, 1996). Orlandi and Fatica (1997), using DNS, added a further contribution by relating the drag reduction to the modifications of the near-wall vortical structures.

Fig. 3 shows the streamwise velocity profile normalized by the wall shear velocity versus the distance from the wall in wall units y^+. Solid lines represent the universal velocity distributions in the viscous sublayer, in the buffer layer and in the inertial sublayer. The viscous sublayer is well resolved in the numerical simulations, yielding the linear velocity distribution $v_z^+ = y^+$ for $y^+ < 5$. The buffer region is also well predicted in accordance with the log-law $v_z^+ = -3.05 + 5 \ln y^+$. The agreement is not so good with the log-law at larger distances from the wall ($y^+ > 30$) for the present LES results as well as for the experimental data by Eggels et al. (1994a). The reason is that the log-laws are not observed in the pipe flow for $Re \leqslant 9600$ ($Re = 2U_b R/\nu$), in contrast to plane channel flow, since the log-law is only justified at large Reynolds numbers (Tennekes and Lumley, 1972). When the pipe rotates, the differences between the computed mean velocity and the log-laws are due to the relaminarization of the flow when increasing N. Similar observations have been reported for the DNS by Orlandi and Fatica (1997). This agrees with most experimental and numerical results (Zhang et al., 1994; Orlandi and Ebstein, 2000).

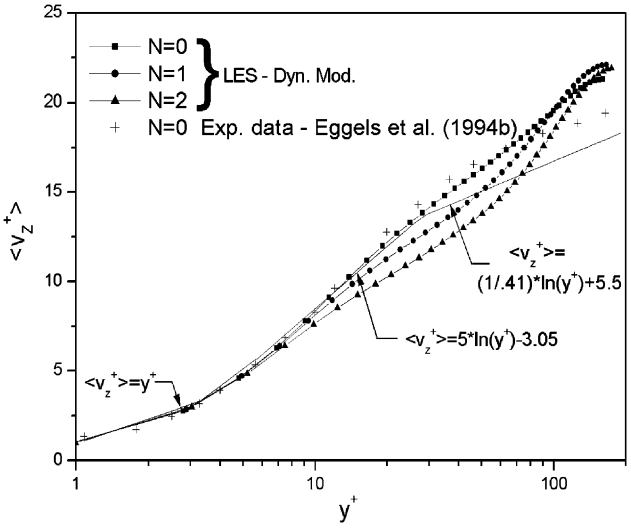

Fig. 3. Axial mean velocity normalized on u_τ as function of the distance (in wall units) from the wall for $Re = 4900$.

The results presented in Figs. 2 and 3 were obtained by using the dynamic subgrid scale model. When using the Smagorinsky model small differences are shown on the mean velocity profile at $Re = 4900$ while noticeable discrepancies are seen about the statistics of turbulence, as it will discussed later on (Fig. 10).

In Fig. 4, two LES computations are presented: the first with the Smagorinsky model and the second with a

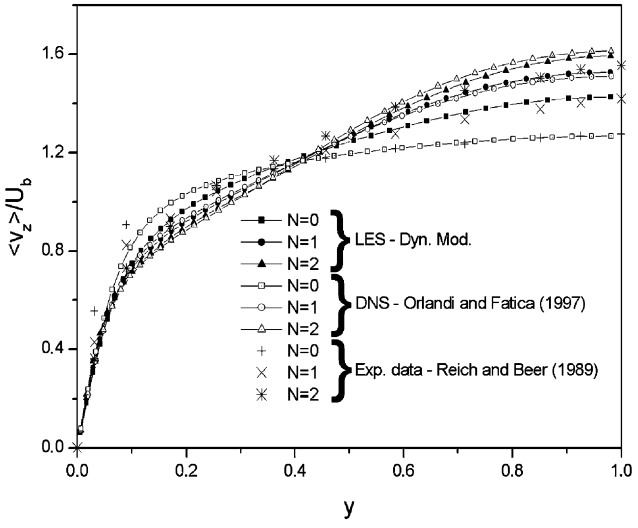

Fig. 2. Axial mean velocity normalized by the bulk velocity U_b as function of the wall distance for $Re = 4900$.

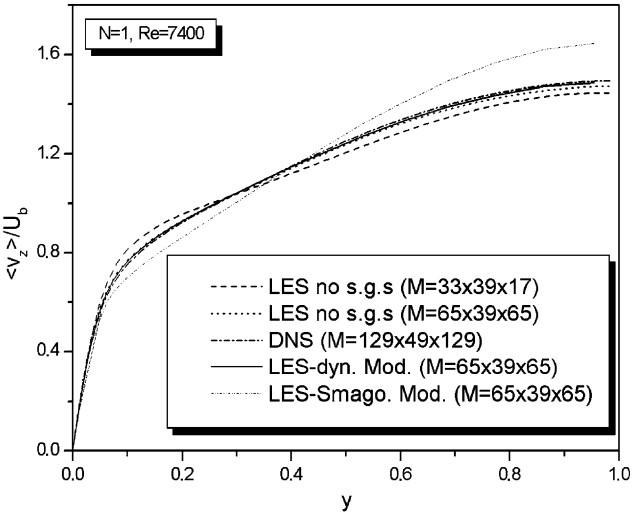

Fig. 4. Axial mean velocity normalized by the bulk velocity U_b as function of the wall distance.

dynamic model. These computations are compared to a DNS prediction as well as to simulations on two coarser grids without subgrid-scale model. The LES profile using a dynamic model is in a good agreement with the v_z-profile predicted by DNS. Additionally, a coarse DNS and a LES with a dynamic model were performed by using the same grid ($65 \times 39 \times 65$). Excellent agreement is obtained applying this LES in comparison with the DNS data base. It seems indeed that the grid scale is much finer than the dominant scales of the flow so that the dynamic model suffices to yield the right behaviour of the dominant scales. Hence, the dynamic subgrid-scale contribution vanishes and the LES turns into DNS. On the other hand, the predictions for the axial velocities using LES with the Smagorinsky model and the simulation without subgrid-scale model do not agree well with the DNS results. Similar conclusion can also be drawn from the results shown in Fig. 5.

The reason of this discrepancy may be the value of the constant C_S of the Smagorinsky model (here $C_S = 0.15$). One of the problems with the Smagorinsky model is that the appropriate value of the coefficient C_S varies according to the flow regimes. In particular, it is zero for laminar flow and it is should be reduced near the walls from its value ($C_S = 0.15$) at high-Reynolds-number free turbulent flows. The Smagorinsky model works well for isotropic turbulence whereas it is too dissipative for inhomogeneous flows because it transfers too much energy to the residual motions (Pope, 2000). For inhomogeneous flows, and in particular for wall bounded flows, the constant C_S has to be modified. For example, C_S was decreased to $C_S = 0.1$ in a channel (Deardorff, 1970; Piomelli et al., 1988) or to $C_S = 0.065$ (Moin and Kim, 1982).

It is worth noting that Mason and Thomson (1992) have studied atmospheric boundary layers and con-

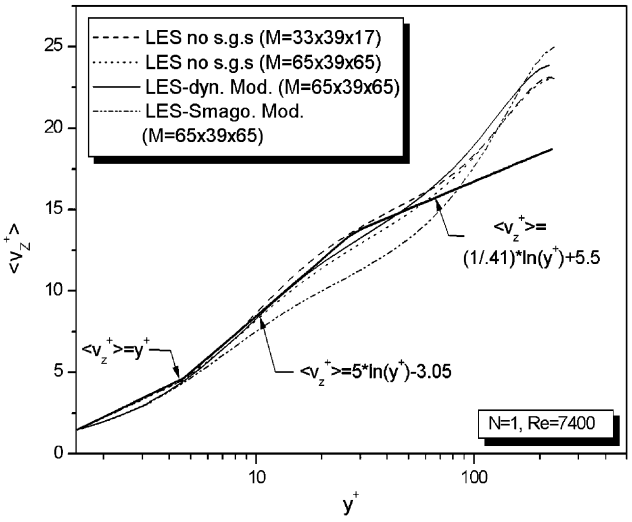

Fig. 5. Axial mean velocity normalized on u_τ as function of the distance (in wall units) from the wall.

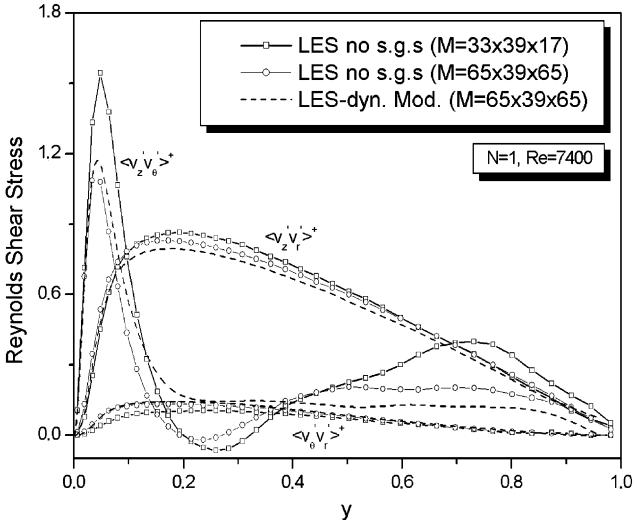

Fig. 6. Reynolds shear–stress in wall units for $N = 1$ and $Re = 7400$.

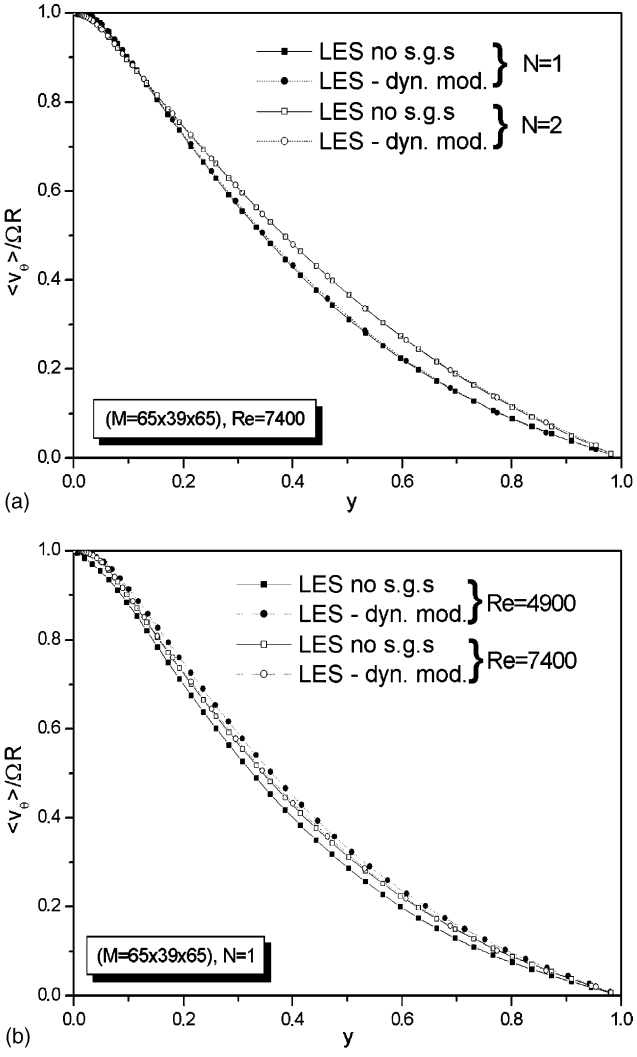

Fig. 7. (a) Tangential mean velocity versus wall distance y for $Re = 7400$. (b) Tangential mean velocity versus wall distance y for $N = 1$.

cluded that the Smagorinsky model is inherently incapable of yielding the correct logarithmic velocity profiles. In addition to these deficiencies, another lack of the Smagorinsky model is that it implies alignment of the turbulent stresses and mean rates of strain. However some numerical (Clark et al., 1979) and experimental (Liu et al., 1994) tests have shown that the alignment is poor. It is important to recognise that the performance of the Smagorinsky model depends on the Reynolds number and on the choice of the type and width of the filter. Thus, it would be very interesting to investigate the influence of these parameters and of the Smagorinsky constant C_S on the statistics in turbulent flows in rotating pipes.

Fig. 6 shows that the LES with the dynamic model leads to closer agreement with the DNS predictions of the Reynolds stresses than the simulation without a subgrid-scale model. The discrepancy is more pronounced for $\langle v'_\theta v'_z \rangle^+$. Therefore, the results shown in Figs. 4–6 emphasise show how important is the subgrid-scale model. In particular the dynamic model is more promising than the Smagorinsky model because there is no adjustable external constant. We conclude then that an appropriate LES gives satisfactory predictions of the rotating pipe flow, and that the subgrid-scale models allows an improvement of the results when coarse grids are used.

Fig. 7 show the mean tangential velocity scaled with the rotating wall velocity versus the wall distance y. In the fully developed flow regime, the tangential velocity profile can be characterised by a parabolic shape (Kikuyama et al., 1983). In the present work, the predictions of the tangential velocity profile were also found to approach a parabolic shape. Such a velocity profile is well predicted by the dynamic model and by DNS. It appears that the effects of the rotation rate and of the Reynolds number on the tangential velocity profile are not very important since v_θ is almost independent of N and Re. Similar observations were reported by Reich and Beer (1989) and by Kikuyama et al. (1983).

Fig. 8 shows that the rotation of the wall at $N = 1$ has large effects on the rms-velocity profile, these effects being more pronounced for the streamwise rms-velocity. Similar observations have been reported by Eggels et al. (1994b) and by Orlandi and Fatica (1997). It can be seen that the fluctuating velocity components obtained with the two subgrid scale models are quite close to those of the DNS, although the results given by the dynamic subgrid scale model are slightly better. The streamwise rms-velocity is presented for various rotation numbers

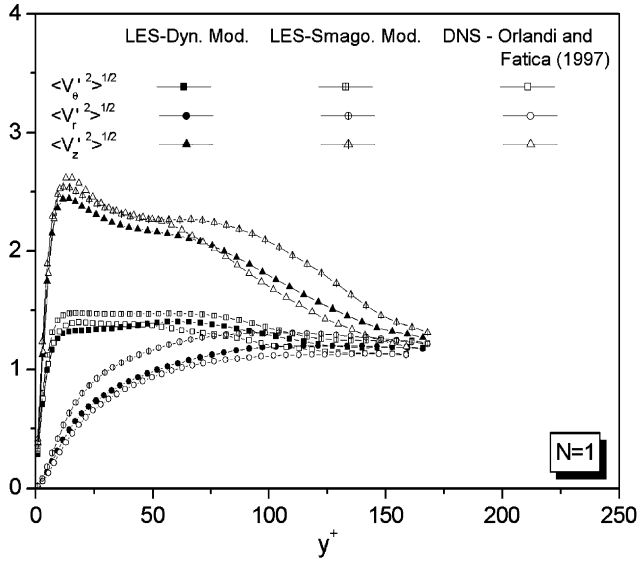

Fig. 8. Root-mean-square (rms) profiles of azimuthal, radial and axial velocity components for $Re = 7400$.

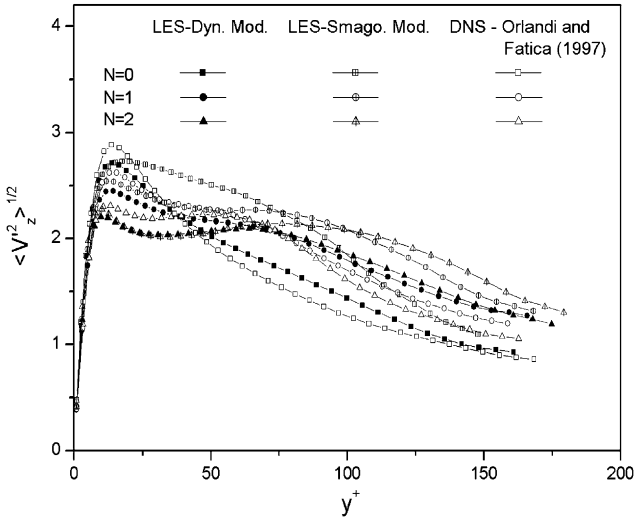

Fig. 9. Rms profiles of axial velocity for $Re = 7400$.

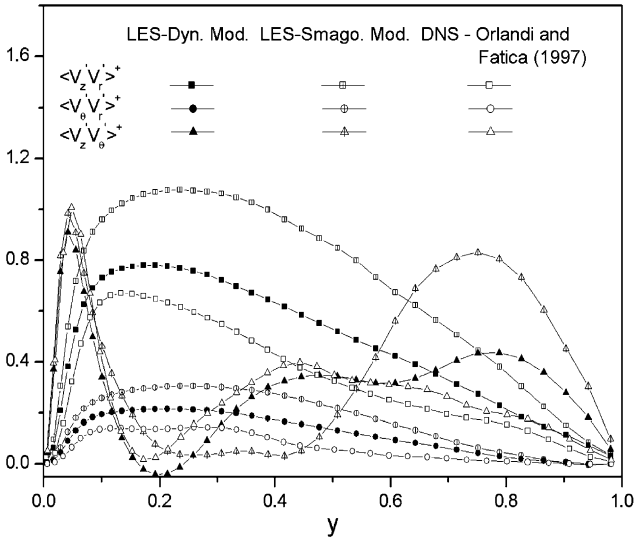

Fig. 10. Reynolds shear stress in wall units for $N = 2$ and $Re = 4900$.

in Fig. 9. Near the wall, the peak is reduced when N increases and the distributions are almost identical in the fully turbulent core region for $N = 2$ and $N = 1$. Orlandi and Fatica (1997) indicate that this tendency is, in a certain sense, an isotropization of turbulence when the rotation rate increases. It should be noted that the distributions of $\langle v_r' 2\rangle^{1/2}$ (or $\langle v_\theta' 2\rangle^{1/2}$) tend also to get the same values when the pipe rotates.

The simulated rms with both subgrid scale models are close to those of DNS but the results calculated using the dynamic subgrid scale model indicate a better agreement. It is worth mentioning however, that there is a large discrepancy in the simulation when using the Smagorinsky model for $N = 0$. The peak in the axial rms profile is obtained but at somewhat larger distance from the wall (at $y^+ \approx 23$); furthermore, the peak is too broad

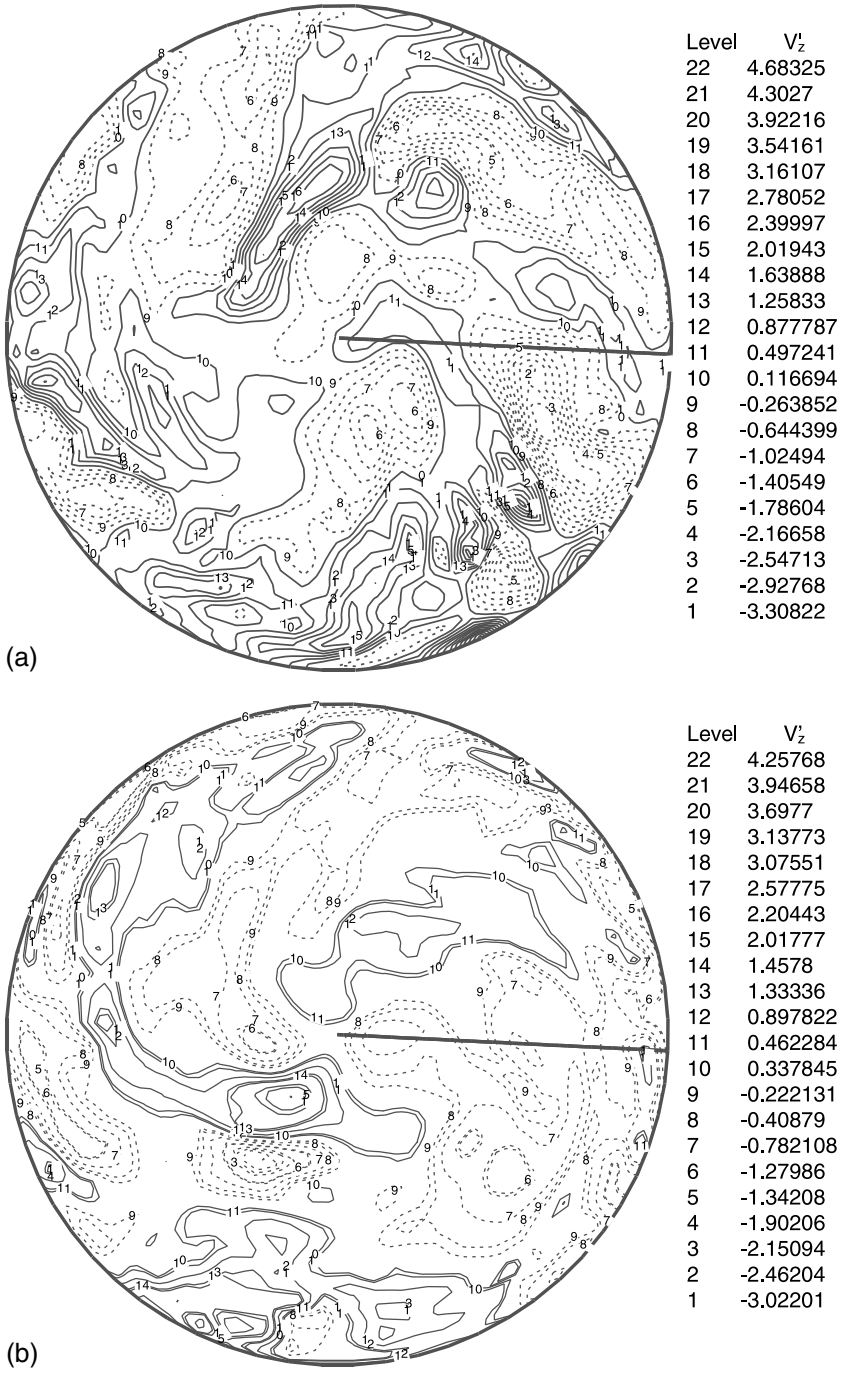

Fig. 11. (a) Contour lines of the axial velocity fluctuations scaled by the rms for $N = 0$ and $Re = 7400$. (b) Contour lines of the axial velocity fluctuations scaled by the rms for $N = 2$ and $Re = 7400$.

in this simulation. Nevertheless, the simulated rms are in reasonable agreement with those computed by Orlandi and Fatica (1997).

The Reynolds shear–stress distributions are shown in Fig. 10 for $N = 2$ at $Re = 4900$. The only non-negligible stress in a non-rotating pipe is $\langle \mathbf{v}'_{\mathbf{r}}\mathbf{v}'_{\mathbf{z}}\rangle^+$. When the pipe rotates, this stress is reduced and the other two stresses $\langle \mathbf{v}'_{\mathbf{r}}\mathbf{v}'_{\boldsymbol{\theta}}\rangle^+$ and $\langle \mathbf{v}'_{\boldsymbol{\theta}}\mathbf{v}'_{\mathbf{z}}\rangle^+$ increase. From Fig. 10, it becomes clear that the three Reynolds stresses are then comparable. Near the rotating wall, the high values of $\langle \mathbf{v}'_{\boldsymbol{\theta}}\mathbf{v}'_{\mathbf{z}}\rangle^+$ are related to the tilting of the near wall vortical structures (Orlandi and Fatica, 1997). In the core region of the flow, the behaviour of $\langle \mathbf{v}'_{\boldsymbol{\theta}}\mathbf{v}'_{\mathbf{r}}\rangle^+$ is almost linear. The Reynolds stresses computed by using the Smagorinsky model are larger than those computed with the dynamic model which are much closer to the DNS stresses.

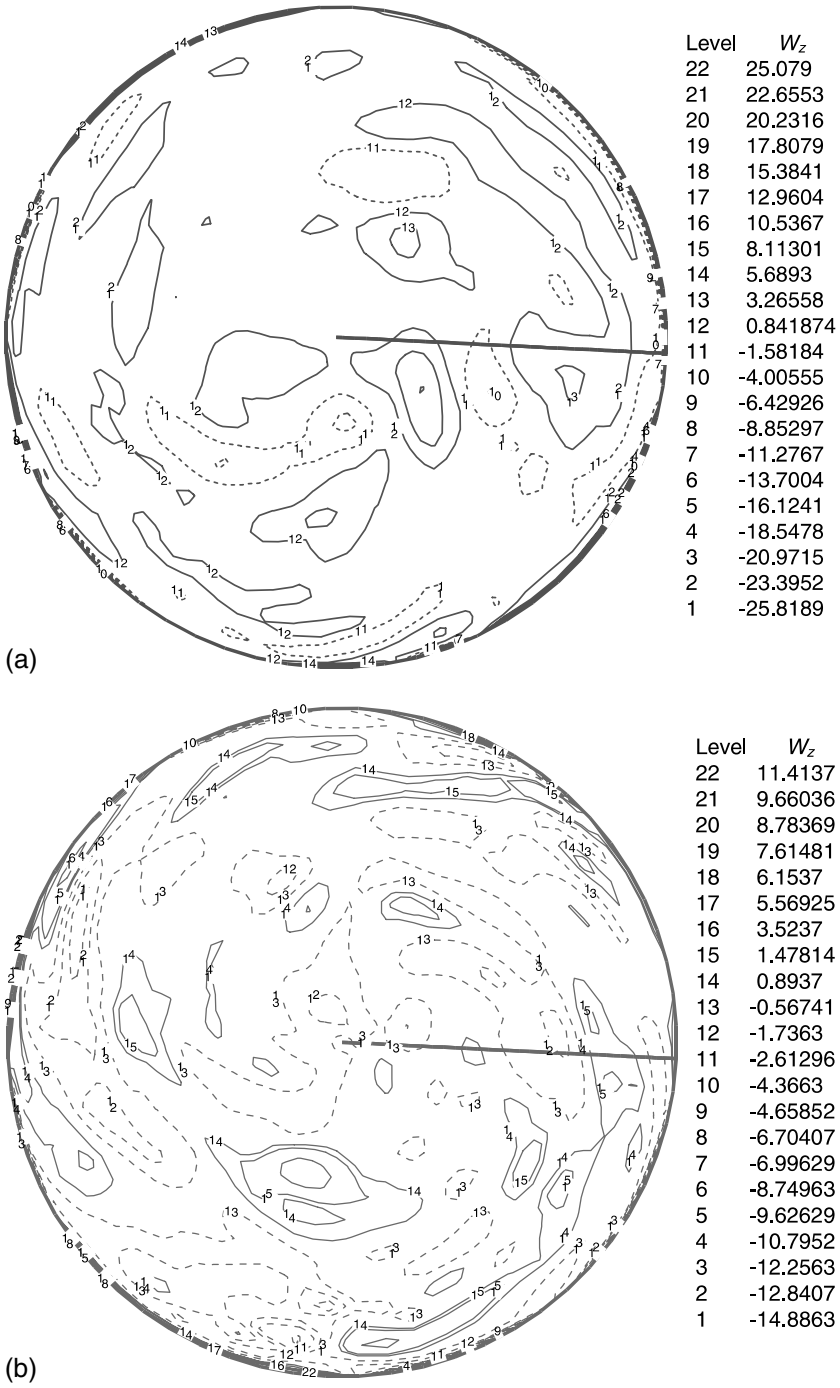

Fig. 12. (a) Contour plot of the axial vorticity component for $N = 0$ and $Re = 7400$. (b) Contour plot of the axial vorticity component for $N = 2$ and $Re = 7400$.

Figs. 11 show contour lines of a snapshot of the axial velocity fluctuations v_z' scaled by the rms value at each r in a plane perpendicular to the axis (r–θ plane), at $N = 0$ (Fig. 11(a)) and at $N = 2$ (Fig. 11(b)) and for $Re = 7400$. These plots present a picture of the turbulent structures (and give an idea of sweep and ejection events). The structures drawn as solid lines correspond to positive values of v_z'. It can be seen the positive v_z' move towards the wall. For a fixed pipe ($N = 0$), the near wall region is dominated by high intensity fluctuations. The sweep events carry high-speed fluid to the wall. For a rotating pipe ($N = 2$) the spreading of the fluid towards the wall is reduced, and very close to the wall there is slightly less turbulent fluctuations (due to the suppression of radial fluctuations). The rotation induce a transport of the fluctuations from the wall towards the central region.

Fig. 12 show contours plots of the axial vorticity component for $N = 0$ (Fig. 12(a)) and $N = 2$ (Fig. 12(b)) at $Re = 7400$. It can be seen that vortical structures exist in certain regions and that the number of structures in the rotating case is larger than for $N = 0$, the intensity of the elongated vortical structures being lower for the rotating pipe.

4. Conclusion

A study of the influence of the rotation number on the fully developed turbulent flow inside an axially rotating pipe was conducted. The simulations were carried out in the same range of rotation numbers and Reynolds numbers as in the DNS by Orlandi and Fatica (1997) who have compared their numerical results with the measurements of Reich and Beer (1989), and with the DNS by Eggels et al. (1994b). The results of the present simulations compare reasonably well with the DNS by Orlandi and Fatica (1997), despite some discrepancies. It is observed that the intensity of turbulence in the rotating pipe decreases gradually with an increase in pipe rotation due to the stabilizing effect of centrifugal forces. We have shown that the dynamic model gives better performance for predicting the fully developed turbulent pipe flow, with or without rotation, than the Smagorinsky model because it is not necessary to specify an external constant according to the rotation speed.

It can be drawn that all phenomena in the rotating and non-rotating turbulent pipe flows can be reasonably captured by LES provided that an appropriate model is retained. This study is a first contribution towards a check of the applicability of the Smagorinsky and the dynamic models to swirling flows.

Acknowledgements

Grant no. 011265 from the IDRIS-computer center (French National Institute for Advances in Scientific Computations) is gratefully acknowledged. Professor P. Orlandi was instrumental in the development of the DNS code employed in this work. The authors wish also to thank the editor and referees for their useful suggestions.

References

Clark, R.A., Ferziger, J.H., Reynolds, W.C., 1979. J. Fluid Mech. 91, 1.
Deardorff, J.W., 1970. J. Fluid Mech. 41, 453.
Eggels, J.G.M., Nieuwstadt, F.T.M., 1993, In: Proc. 9th Symp. on Turbulent Shear Flows, Kyoto, Japan, p. 310.
Eggels, J.G.M., Boersma, B.J., Nieuwstadt, F.T.M., 1994a, Preprint.
Eggels, J.G.M., Unger, F., Weiss, F.M.H., Westerweel, J., Adrian, R.J., Friedrich, R., Nieuwstadt, F.T.M., 1994b. J. Fluid Mech. 268, 175.
Germano, M., Piomelli, U., Cabot, W.H., 1991. Phys. Fluids A 3, 1760.
Hirai, S., Takagi, T., Matsumoto, M., 1988. Trans. ASME J. Fluids Engng. 110, 424.
Imao, S., Itoh, M., 1996. Int. J. Heat Fluid Flow 17, 444.
Itoh, N., 1977. J. Fluid Mech. 82, 469.
Kikuyama, K., Murakami, M., Nishibori, K., 1983. Bull. JSME 26, 506.
Laufer, J., 1954. NACA Report 1174.
Lawn, C.J., 1971. J. Fluid Mech. 48, 477.
Lilly, D.K., 1992. Phys. Fluids A 4, 633.
Liu, S., Meneveau, C., Katz, J., 1994. J. Fluid Mech. 275, 83.
Mason, P.J., Callen, N.S., 1986. J. Fluid Mech. 162, 439.
Mason, P.J., Thomson, D.J., 1992. J. Fluid Mech. 242, 51.
Moin, P., Kim, J., 1982. J. Fluid Mech. 118, 341.
Nikitin, N.V., 1993. Bull. APS 38 (12), 2311.
Nishibori, K., Kikuyama, K., Murakami, M., 1987. JSME Int. J. 30, 255.
Orlandi, P., Fatica, M., 1997. J. Fluid Mech. 143, 43.
Orlandi, P., Ebstein, D., 2000. Int. J. Heat Fluid Flow 21, 499.
Patera, A.T., Orszag, S.A., 1981. J. Fluid Mech. 112, 467.
Piomelli, U., Moin, P., Ferziger, J.H., 1988. Phys. Fluids 31, 1884.
Pope, S.B., 2000. Turbulent flows. Cambridge University Press.
Reich, G., Beer, H., 1989. Int. J. Heat Mass Transfer 32, 551.
Tennekes, H., Lumley, J.L., 1972. A First Course in Turbulence. MIT Press.
Unger, F., Eggels, J.G.M., Friedrich, R., Nieuwstadt, F.T.M., 1993. In: Proc. 9th Symp. on Turbulent Shear Flows, Kyoto, Japan, p. 2/1/1-2/1/6.
Unger, F., Friedrich, R., 1991. In: Proc. 8th Symp. on Turbulent Shear Flows, Munich, Germany, pp. 19-3-1–19-3-6.
Yang, Z., McGuirk, J.J., 1999. In: Proc. Turbulence and Shear Flow Phenomena, USA, p. 863.
Zhang, Y., Gandhi, A., Tomboulides, A.G., Orszag, S.A., 1994. In: AGARD Conf. Proc., 551, pp. 17.1–17.9.